

RESEARCH ARTICLE

10.1029/2017JD028012

Key Points:

- Assimilation of LPW from AHI shows substantial improvement on heavy precipitation forecasts over that from conventional data
- Comparison between AHI radiance and LPW assimilation shows improved impact from LPW, partly due to limited radiance assimilation over land
- This study provides an alternative way of assimilating high-resolution moisture information from the advanced imagers onboard GEO satellites

Correspondence to:

J. Lu,
lujz1969@126.com

Citation:

Wang, P., Li, J., Lu, B., Schmit, T. J., Lu, J., Lee, Y.-K., et al. (2018). Impact of moisture information from advanced Himawari imager measurements on heavy precipitation forecasts in a regional NWP model. *Journal of Geophysical Research: Atmospheres*, 123, 6022–6038. <https://doi.org/10.1029/2017JD028012>

Received 7 NOV 2017

Accepted 24 MAY 2018

Accepted article online 31 MAY 2018

Published online 12 JUN 2018

Impact of Moisture Information From Advanced Himawari Imager Measurements on Heavy Precipitation Forecasts in a Regional NWP Model

Pei Wang¹ , Jun Li¹ , Bing Lu², Timothy J. Schmit³ , Jiazhen Lu⁴, Yong-Keun Lee¹ , Jinlong Li¹ , and Zhiqian Liu⁵ 

¹Cooperative Institute for Meteorological Satellite Studies, University of Wisconsin-Madison, Madison, WI, USA, ²Institute of Urban Meteorology, China Meteorological Administration, Beijing, China, ³Center for Satellite Applications and Research, NESDIS/NOAA, Madison, WI, USA, ⁴State Key Laboratory of Disaster Prevention and Reduction for Power Grid Transmission and Distribution Equipment, Changsha, China, ⁵National Center for Atmospheric Research, Boulder, CO, USA

Abstract Information about moisture distribution and transportation in the preconvective environment is very important for nowcasting and forecasting severe weather events. The Advanced Himawari Imager (AHI) onboard the Japanese Himawari-8/9 provides high temporal and spatial resolution moisture information useful for weather monitoring and forecasting. Algorithms have been developed for three-layered precipitable water (LPW: surface to 0.9, 0.9–0.7, and 0.7–0.3 in sigma vertical coordinate) retrievals from AHI infrared band radiances using a Geostationary Operational Environmental Satellite-R series algorithm working group algorithm. The LPW products from AHI have been validated with in situ measurements. An important application of the AHI LPW product is to improve local severe storm forecasts through assimilating high temporal and spatial resolution moisture information into regional- and storm-scale numerical weather prediction (NWP) models. Assimilation techniques and approaches have been developed; the impact on precipitation forecasts for local severe storm over land from the assimilation of LPWs from AHI shows improvement on heavy precipitation forecasts over those from the assimilation of conventional data. Comparisons between AHI infrared band radiance assimilation and LPW assimilation show overall similar or comparable impact on precipitation forecast. The approaches for assimilating LPW can be applied to the assimilation of data from other advanced imagers such as the Advanced Baseline Imager onboard the U.S. next generation of Geostationary Operational Environmental Satellites-R series, the Advanced Geosynchronous Radiation Imager onboard the Chinese FengYun-4 series, and the Flexible Combined Imager onboard the upcoming European Meteosat Third Generation.

1. Introduction

Information about moisture distribution and transportation in the preconvective environment is very important for nowcasting and forecasting severe weather events (Lee et al., 2017; Li et al., 2008, 2011, 2012; Sieglaff et al., 2009; Weisz et al., 2015). The Advanced Baseline Imager (ABI) onboard the U.S. next generation of Geostationary Operational Environmental Satellite (GOES-R series; Schmit et al., 2005, 2008, 2017), the Advanced Himawari Imager (AHI) onboard the Japanese Himawari-8/9 (Bessho et al., 2016), and the Advanced Geosynchronous Radiation Imager (AGRI) onboard the Chinese FengYun-4 series (Yang et al., 2017) provide high temporal (30 s to 15 min) and spatial (2 km for ABI and AHI and 4 km for AGRI; Table 1) resolution moisture information useful for weather monitoring and forecasting. Algorithms have been developed for three-layered precipitable water (LPW: surface to 0.9, 0.9–0.7, and 0.7–0.3 in sigma vertical coordinate) retrievals by combining the ABI/AHI infrared (IR) band radiances, numerical weather prediction (NWP) model moisture forecasts, and surface temperature and moisture observations (Jin et al., 2008; Li et al., 2009). The LPW products from ABI/AHI have been validated with in situ measurements (Lee et al., 2014), generated at the Space Science and Engineering Center (SSEC) at the University of Wisconsin-Madison, and put into the Advanced Weather Interactive Processing System-II in near real time to allow forecasters to monitor a critical ingredient in the initiation, development, and decay of convective cells and systems (Li et al., 2008, 2009). These unique LPW products can depict high temporal and spatial features such as a dry line. Examples from the National Oceanic and Atmospheric Administration (NOAA) Hazardous

Table 1
The Central Wavelength and Spatial Resolution of AHI/ABI/AGRI Bands

Himawari-8/AHI			GOES/ABI			FY-4A/AGRI		
Band	Central wavelength (μm)	Spatial resolution (km)	Band	Central wavelength (μm)	Spatial resolution (km)	Band	Central wavelength (μm)	Spatial resolution (km)
1	0.46	1	1	0.47	1	1	0.46	1
2	0.51	1	2	0.64	0.5	2	0.64	0.5~1
3	0.64	0.5	3	0.86	1	3	0.86	1
4	0.86	1	4	1.37	2	4	1.38	2
5	1.6	2	5	1.6	1	5	1.61	2
6	2.3	2	6	2.2	2	6	2.25	2~4
7	3.9	2	7	3.9	2	7	3.80 (high)	2
8	6.2	2	8	6.29	2	8	3.80 (low)	4
9	7	2	9	6.9	2	9	6.5	4
10	7.3	2	10	7.3	2	10	7.2	4
11	8.6	2	11	8.4	2	11	8.5	4
12	9.6	2	12	9.6	2			
13	10.4	2	13	10.3	2			
14	11.2	2	14	11.2	2	12	11	4
15	12.3	2	15	12.3	2	13	12	4
16	13.3	2	16	13.3	2	14	13.3	4

Note. AHI = Advanced Himawari Imager; ABI = Advanced Baseline Imager; AGRI = Advanced Geosynchronous Radiation Imager; GOES = Geostationary Operational Environmental Satellite; FY-4A = FengYun-4 series.

Weather Testbed which occurred 4 May to 12 June 2015, 18 April to 13 May 2016, and 1 May to 2 June 2017 have demonstrated the forecast applications of these very useful products.

Another important application is to improve tropical cyclone (TC) and local severe storm (LSS) forecasts through the assimilation of high temporal and spatial resolution moisture information into global-, regional-, and storm-scale NWP models. For TCs, vertical water vapor information from the advanced IR sounder onboard NASA's Earth Observing System satellite Aqua can improve the hurricane path and intensity predictions (Li & Liu, 2009; Liu & Li, 2010). For LSS, studies have shown that assimilation of the current GOES Imager IR radiances improves the coastal precipitation forecasts (Qin et al., 2013; Zou et al., 2011) and TC forecasts (Zhang et al., 2016), although the data used over land are limited (Zou et al., 2011). Qin et al. (2017) also found that AHI provided more improvements in precipitation forecasts when assimilated than the current GOES-like imager radiances due to two additional water vapor absorption bands on AHI. Ma et al. (2017) assimilated AHI radiances in NOAA's global forecast system (GFS) and found that IR water vapor channels and atmospheric motion vectors, in addition to the current global observing system, show neutral to marginal positive impact on analysis and forecast skill relative to assimilation without AHI data. The main positive impact occurs for short- to medium-range forecasts of global upper-tropospheric water vapor.

In this study, the assimilation of total precipitable water (TPW) from satellites (Deblonde, 1999; Hou et al., 2000; Rakesh et al., 2009) is extended to the assimilation of three LPWs from AHI. The assimilation experiments are conducted on NOAA/National Environmental Satellite, Data, and Information Service (NESDIS)/Center for Satellite Applications and Research (STAR) Supercomputer for Satellite Simulations and data assimilation Studies (S4; Boukabara et al., 2016) physically located at SSEC on the University of Wisconsin-Madison campus, using the advanced research version of the Weather Research Forecast (WRF-ARW) model and the community Gridpoint Statistical Interpolation (GSI) three-dimensional incremental variational (3Dvar) system. A forward operator for LPWs has been developed and implemented into the GSI system, and tools have also been developed to convert the LPW data to the format that GSI uses. LPW research products from AHI are produced at SSEC by using a similar GOES-R ABI algorithm.

The 19–20 July 2016 Beijing storm and the mid-June 2016 Yangtze River heavy rainfall cases are studied by using WRF/GSI system. The issue of radiance versus retrieval assimilation has been previously investigated,

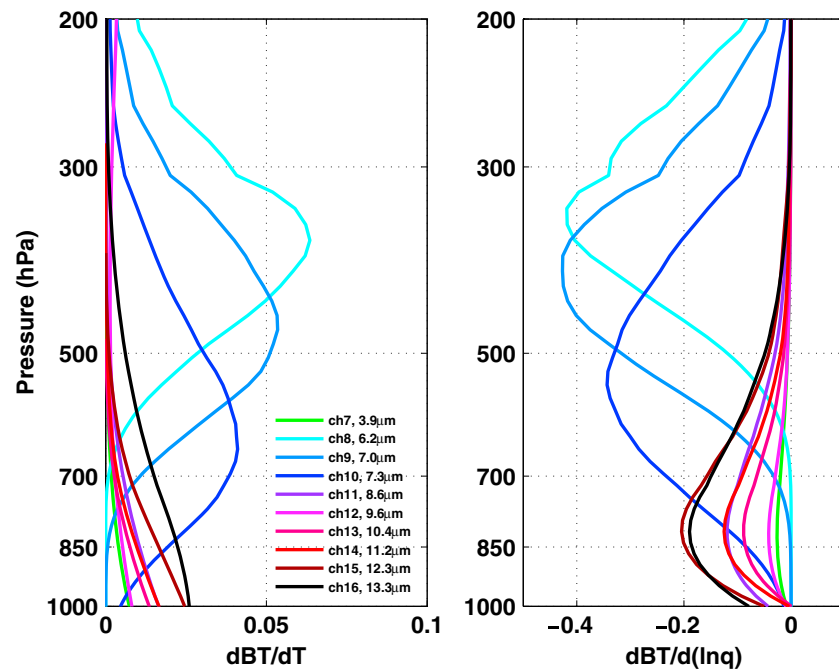


Figure 1. The weighting function of AHI IR bands from 8 to 10 and 13 to 16 calculated with CRTM. AHI = Advanced Himawari Imager; IR = infrared; CRT = community radiative transfer model.

and assimilating transformed retrievals may be particularly advantageous for sensors with a very high number of spectral channels (Migliorini, 2012). Most global NWP centers use direct assimilation of radiances, based on the successes at both the National Centers for Environmental Prediction (NCEP) and the European Center for Medium-Range Weather Forecasting. However, due to the challenge of assimilating moisture information in NWP, it is worthwhile to study the assimilation of three LPWs and to obtain value-added information from these advanced imagers, such as AHI and ABI, into NWP.

Section 2 provides an overview of the LPW retrieval methodologies and validation. Section 3 presents the impact from LPW assimilation for typical heavy rainfall cases. Section 4 compares the LPW assimilation and the radiance assimilation on precipitation forecasts. Section 5 provides a summary and discussion.

2. AHI LPW Algorithm and Validation

The weighting functions of AHI IR bands calculated from the U.S. standard atmosphere with the NOAA Joint Center for Satellite Data Assimilation community radiative transfer model (CRTM) are shown in Figure 1. The temperature and moisture weighting functions of each spectral band reflect the temperature and water vapor information layers, respectively. The peak and the depth of information layers depend on the atmospheric conditions (Di et al., 2016), which form the basis for retrieving LPW information from radiance measurements in clear skies. The retrieval algorithm and software have been developed to retrieve LPW from advanced imagers such as the ABI onboard the new generation U.S. GOES-R series, AHI onboard the Japanese Himawari-8 and Himawari-9 satellites, and AGRI onboard the Chinese FengYun-4 series. It retrieves the legacy atmospheric temperature and moisture profiles from the clear-sky IR radiances within an M by M field of view box area; a priori profile information from NWP short-range forecasts (9–12 hr) is used as the background and first guess. CRTM and its associated Jacobian are used in a one-dimensional variational (1DVAR)-based retrieval algorithm (Jin et al., 2008; Li et al., 2000). In the AHI processing, $M = 5$ is used. TPW, LPW, lifted index (LI), convective available potential energy, total totals index, Showalter index, and K index are derived from the retrieved temperature and moisture profiles. The profile product generation requires IR brightness temperatures (BTs) from eight AHI IR channels (excluding 3.9- and 9.6- μm channels) along with the NWP background. The LPWs at three atmospheric layers in sigma vertical ordinate (PW_low: 0.9 to surface (SFC), PW_mid: 0.7–0.9, and PW_high: 0.3–0.7) are produced. The model top is

0.005 hPa. The sigma vertical coordinate for the atmospheric model is defined by the normalized pressure at the surface. LPW is defined as the amount of liquid water (in mm) if all the atmospheric water vapor in the layer is condensed. The following equation is used to derive LPW:

$$LPW = \frac{10}{\rho_w g} \sum_{k=1}^n 0.5 \cdot (q(k+1) + q(k)) \cdot (p_k - p_{k+1}) \quad (1)$$

where ρ_w equals 1,000 which is the water density in kg/m^3 , g is the gravity acceleration in m/s^2 , $q(k)$ is the mixing ratio (g/kg) of the water vapor profile at the k th level, and $p_{k=1}$ is the lower level air pressure of the atmospheric layer in hPa. $p_{k=n}$ is the upper level air pressure of the atmospheric layer in hPa. Equation (1), along with its linear form, is also the forward operator for assimilating LPW, and the GSI has been modified to include the above LPW operator for assimilation.

In some cases, such as the center of a low-pressure system, the surface air pressure could be lower than 900 hPa. In other cases, such as over high-altitude areas, the surface pressure can be lower than 700 hPa, and therefore, the sigma pressure coordinate is applied to circumvent such cases. The boundaries for PW calculation are converted into sigma indices with the values of 1.0, 0.9, 0.7, and 0.3, respectively. The following equation describes the conversion between sigma pressure and normal air pressure ordinate

$$P_{\text{sig}} = 0.005 + \text{sig_idx} \cdot (P_s - 0.005) \quad (2)$$

where P_{sig} is the pressure corresponding to a specific sigma level index, sig_idx is the sigma index, and P_s is the surface air pressure. Since the retrieved moisture profile does not necessarily contain values at these levels for different surface pressures, a linear interpolation is conducted to find mixing ratio values at these levels:

$$q(p_{\text{sig}}) = q(p_{\text{below}}) + [q(p_{\text{above}}) - q(p_{\text{below}})] \cdot \left[\frac{\ln q(p_{\text{sig}}) - \ln q(p_{\text{below}})}{\ln q(p_{\text{above}}) - \ln q(p_{\text{below}})} \right] \quad (3)$$

where q is the mixing ratio profile, p_{above} is the pressure level just above p_{sig} , and p_{below} is the pressure level just below p_{sig} . The detailed algorithm for LPW retrieval from geostationary advanced imagers can be found in Jin et al. (2008) and the ABI Algorithm Theoretical Basis Document (www.goes-r.gov).

Validation of TPW and LPW has been conducted by comparing retrievals with different reference measurements such as radiosonde observations and the microwave radiometer-measured TPW at the Atmospheric Radiation Measurement Cloud and Radiation Testbed site, TPW measurements from the global positioning system-integrated precipitable water NOAA network, and TPW measurements from the Advanced Microwave Scanning Radiometer for Earth Observing System. Results show that the TPW and LPW are more accurate and precise than GFS short-range (9–12 hr) forecasts, especially for water vapor between 300 and 700 hPa. Detailed validation procedures and results can be found in Lee et al. (2014).

3. Assimilation and Impact Study

3.1. Data Assimilation System and the NWP Model

GSI is a data assimilation system designed for both global and regional models (Kleist et al., 2009; Wu et al., 2002). It is primarily a 3Dvar system, and it has the option to be used as a hybrid data assimilation system as well (Wang et al., 2013). It was developed jointly by NOAA, National Aeronautics and Space Administration, and National Center for Atmospheric Research and has been used as an operational model in the NCEP global model (Global Data Assimilation System), North American Mesoscale Forecast System, Hurricane WRF, Rapid Refresh, and other models. The Developmental Testbed Center transitioned the operational GSI system into a community version for research, real-time models (i.e., CIMSS Satellite Data Assimilation for Tropical storm forecasts: <http://cimss.ssec.wisc.edu/sdat>), and case studies. Because GSI can assimilate many types of observations (i.e., conventional data, satellite radiances, and radar data), it has been widely used in the research community (Han et al., 2016; Lim et al., 2014; Qin et al., 2013, 2017; Wang et al., 2014, 2015; Zou et al., 2011). Version 3.3 of the Developmental Testbed Center-GSI is used as the data assimilation system in this study. Due to limited resources in generating the ensemble members for hybrid assimilation in regional

models, the 3DVAR method is applied to assimilate the data and study the data impacts. For satellite radiance assimilation, a forward radiative transfer model is required to simulate the radiance from the background. CRTM is implemented in GSI for satellite radiance simulation and assimilation (Chen et al., 2010, 2012; Han et al., 2006). The coefficients from CRTM version 2.1.3 are used in this study.

The WRF-ARW is a community mesoscale model developed by NCAR. This study used version 3.6.1 of the WRF-ARW. Since first released, the WRF-ARW continues to be updated every year to implement additional physical schemes for research and case studies. It is also used as an NWP model in operational centers and near-real-time systems, such as Rapid Refresh and Satellite Data Assimilation for Tropical storm forecasts. The final (FNL) reanalysis data from the NCEP GFS model are used as initialization and boundary layer conditions in this regional NWP simulation. The resolution of FNL data is $1^\circ \times 1^\circ$ with global coverage. Some of the physics schemes used in the following case studies include the following: WSM6 (Hong & Lim, 2006) is used as the microphysics scheme, the YSU (Hong et al., 2006) scheme is the PBL physics scheme, the cumulus parameterization is from Kain-Fritsch (Kain, 2004) and was only applied to domain 1, and the RRTMG (Iacono et al., 2008) is used as both longwave and shortwave physics schemes.

3.2. Case I: 19–20 July 2016 Beijing Storm

Heavy rain occurred from 19 to 20 July 2016 in Beijing with average rainfall of 212.6 mm from all monitoring stations: 274 mm over the urban area, 259.8 mm over the southwest, 217.7 mm over the southeast, 200.7 mm over the northwest, and 144.1 mm over the northeast. The heaviest rainfall, 453.7 mm, was observed at Dongshan Village of the Mentougou District. Overall, 362 stations observed rainfall of more than 100 mm, 125 stations observed more than 250 mm, and 4 stations observed more than 400 mm. This persistent heavy rain caused widespread disruption in the Chinese capital, Beijing, forcing the delay and cancellation of hundreds of flights and the closure of some subway stations. The Beijing city government issued an orange alert, the second highest in China's four-tier warning system. Figure 3 (upper left) gives the accumulated rainfall of observation from 1800 UTC 18 July to 1800 UTC 19 July 2016. The observation precipitation data are from China's hourly merged precipitation analysis combining observations from automatic weather stations with CMORPH at $0.1^\circ \times 0.1^\circ$ grid (Shen et al., 2014).

In order to study the impact of AHI LPW on such heavy rainfall forecasts, the LPWs retrieved from Himawari-8 AHI in clear skies are prepared for assimilation, with the GOES-R algorithm working group team algorithm (Heidinger et al., 2013) applied to AHI data for cloud detection. Two nested domains with horizontal resolution of 12 and 4 km, respectively, and 51 vertical layers from surface to 10 hPa, are used in WRF-ARW v3.6.1. Domain 1 has 400×250 grid points, and domain 2 has 601×400 grid points. The LPW assimilation is adopted within the large domain (domain 1) with a North American Mesoscale Forecast System background error covariance matrix.

The assimilation and forecast experiments began at 0000 UTC on 18 July 2016, with a 6-hr spin-up forecast as a warm start for the data assimilation. The data are assimilated at 0600 UTC on 18 July and 1200 UTC on 18 July, followed by a 48-hr forecast from 1200 UTC on 18 July to 1200 UTC on 20 July 2016. The conventional data from the global telecommunication system (GTS) and LPW data retrieved from AHI are assimilated in the study. The assimilation window is ± 3 hr for GTS data and ± 0.5 hr for LPW. The LPW retrieval algorithm and preliminary evaluations can be found in Jin et al. (2008) and Lee et al. (2014). Based on our further comparisons among AHI LPW, radiosonde observations, and GPS PW data, LPW observation errors are set at 1.16 mm for low-layer PW, 1.75 mm for middle-layer PW, and 1.22 mm for high-layer PW in this study. It should also be noted that slight changes in these errors are not very sensitive to the FNL data impacts during our test. In general, the ratio of assimilated observations to the total number of available observations is between 50% and 60%. The following lists the experiments developed to study LPW data impacts:

1. CNTRL: GTS (all conventional data from the GTS)
2. LPW (H): GTS + high-layer PW (from 0.3 to 0.7 sigma level)
3. LPW (M): GTS + middle-layer PW (from 0.7 to 0.9 sigma level)
4. LPW (L): GTS + low-layer PW (from 0.9 sigma level to surface)
5. LPW (HM): GTS + high-layer PW + middle-layer PW
6. LPW (ML): GTS + middle-layer PW + low-layer PW

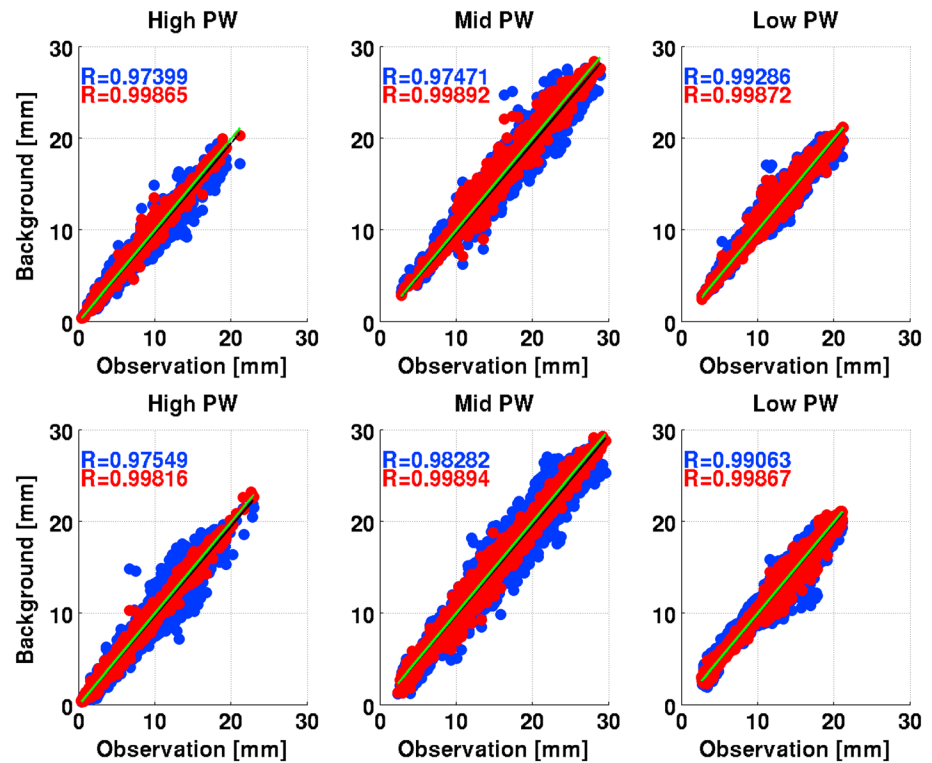


Figure 2. The three-layered precipitable water (high PW, middle PW, and low PW) against background (blue dots) and analysis (red dots) with slope lines at 0600 UTC on 18 July 2016 (upper panel) and 1200 UTC on 18 July 2016 (lower panel). The numbers of R and the solid lines give the slope of the scatter dots. PW = precipitable water.

7. LPW (HL): GTS + high-layer PW + low-layer PW
8. LPW (HML): GTS + three-layered PW

Figure 2 shows LPW (HML) containing all three-layered PW data, the background, and analysis fields against observations (upper panel) at 0600 UTC on 18 July. The observations versus background are identified with blue dots and a black slope line, and the observations versus analysis are identified with red dots and a green slope line. The sample size is 3,746. Figure 2 (lower panel) shows the layered PW data at 1200 UTC on 18 July with a sample size of 4,932. Based on the slope line and the data distribution, the analysis fields have smaller differences in relation to the observations than the background fields, which indicates that the implemented module can assimilate LPW well in the GSI system. The assimilated LPW data can change the analysis moisture fields and then affect the LSS forecast results.

Figure 3 shows the 24-hr accumulated precipitation from CNTRL and assimilated LPW (HML), respectively, along with the observations. In general, the precipitation patterns from the two experiments are similar to the observations. However, the heavy rainfall locations for the two experiments are different. For example, observed rainfall greater than 120 mm (the black box region) covers from 35°N to 39°N, while the heavy rainfall from CNTRL is found from 35°N to 37.5°N, and there is heavy precipitation on the western side of the box region, which is different from the observations. Compared to CNTRL, the precipitation pattern from assimilating LPW (HML) is closer to the observations, which indicate weak precipitation on the western side of the box region and strong precipitation from 35°N to 38.535°N (see the differences between CNTRL and LPW experiments in the upper right panel of Figure 3). ETS (equitable threat score) is calculated for the 24-hr cumulative precipitation forecasts (Figure 3 lower figure). From 0.1 to 75 mm, the ETS of assimilation of LPW (HML) is higher than CNTRL, especially for 1-, 5-, and 10-mm precipitation forecast. To further quantitatively verify the precipitation forecasts, the mean and STD between experiences and the observations are calculated. The mean value between the CNTRL and observations is -2.5537 mm, and the STD is 37.0476 mm; the mean value between assimilation of LPW and observations is -2.1791 mm, and the STD is 34.0674 mm. The STD between CNTRL and observations in the black box is 96.4537 mm, and the STD between LPW (HML)

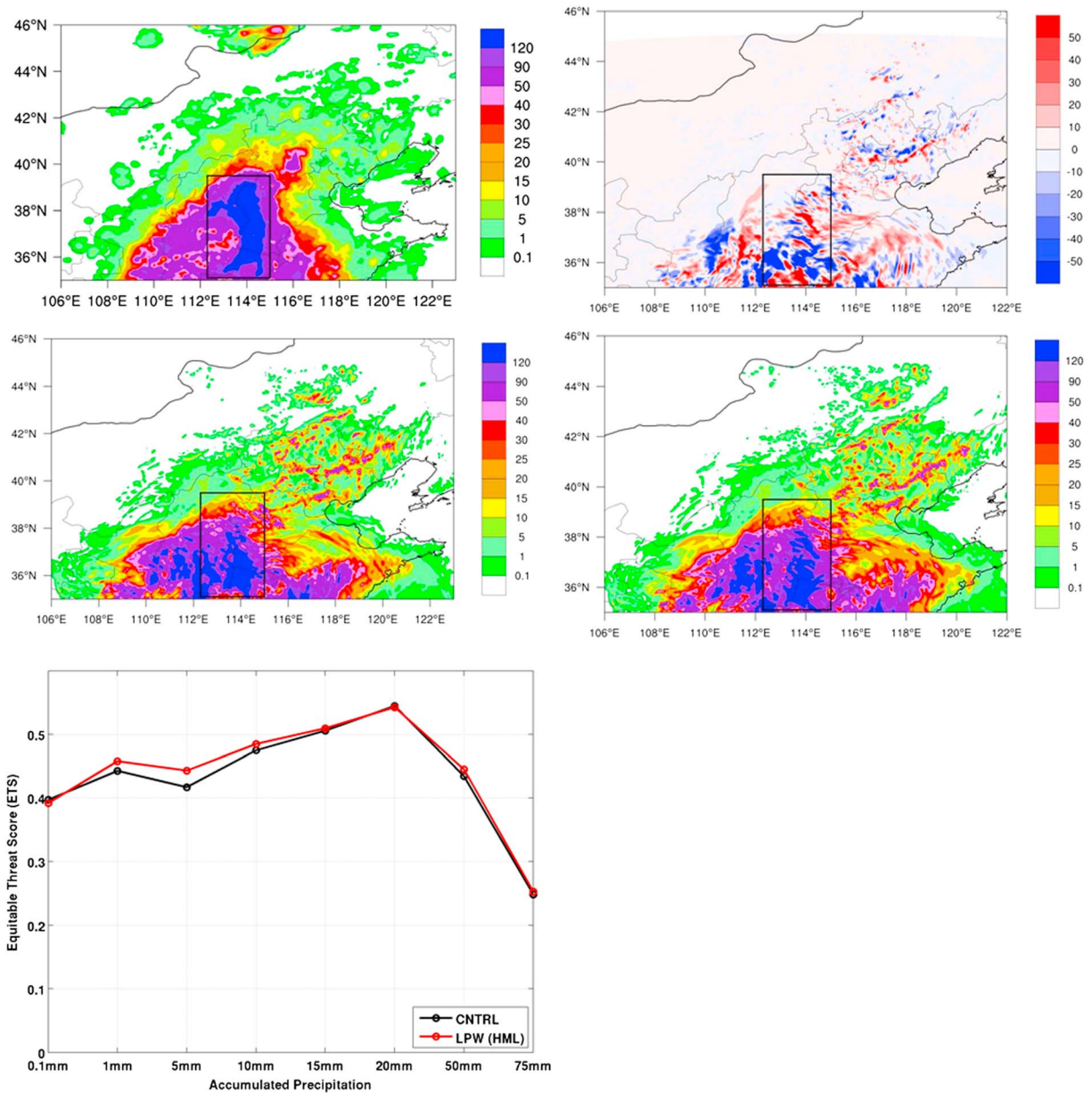


Figure 3. The 24-hr accumulated rainfall for Beijing 7.19/20 LSS case from observations (upper left), CNTRL (middle left), and LPW (HML; middle right), the rainfall difference between CNTRL and LPW (HML; upper right), and ETS of the 24-hr forecasts (lower) from 1800 UTC on 18 July to 1800 UTC on 19 July 2016. LSS = local severe storm; LPW = layered precipitable water.

and observations in the black box is 82.3816 mm. There is about a 15% reduction in STD with the assimilation of LPW data. Both the mean and STD show that the assimilation of LPW data can reduce the precipitation forecast error by incorporating accurately observed moisture information into the model system.

To further evaluate the impacts of assimilating LPW data on Beijing LSS forecasts, an ETS, the probability of detection (POD), and the false alarm ratio (FAR) scores are calculated for all of the experiments. An ETS score can be used to evaluate nonprobabilistic, gridded precipitation forecasts (Ebert et al., 2007; Hamill, 1999). Based on Table 2, ETS can be defined as

$$ETS = \frac{\text{Hits} - \text{Hits random}}{\text{Hits} + \text{Misses} + \text{False Alarms} - \text{Hits random}}$$

Table 2
Contingency Table Used in Verification Statistics for Dichotomous (et. Yes/No) Forecasts and Observations

Forecast	Observation		
	Yes	No	
Yes	Hits (YY)	False alarms (YN)	YY + YN
No	Misses (NY)	correct rejections (NN)	NY + NN
	YY + NY	YN + NN	Total = YY + YN + NY + NN

$$\text{where Hits random} = \frac{(\text{Hits} + \text{False Alarms})(\text{Hits} + \text{Misses})}{\text{Total}}$$

POD = $\frac{\text{Hits}}{\text{Hits} + \text{Misses}}$, which gives the fraction of rain occurrences that were correctly detected. FAR = $\frac{\text{False Alarms}}{\text{Hits} + \text{False Alarms}}$, which measures the fraction of rain detections that were false alarms.

The forecast precipitation for all of the experiments is compared with observations, after which the ETS scores for each experiment are calculated. The resolution of the observed precipitation is $0.1^\circ \times 0.1^\circ$ grid, which is coarser than the 4-km resolution of domain

2. The forecast precipitation is interpolated to the observation grid points and then the ETS equation is applied to calculate the precipitation inside a box from 35°N to 46°N latitude and from 106°E to 122°E longitude. The ETS scores from all of the experiments with rainfall greater than or equal to 10 mm are calculated in Table 3. The accumulated precipitation starts from 1200 UTC 18 July 2016. ETS scores in red are higher than those in the experiment assimilating GTS conventional data only. Numbers in bold indicate the highest ETS scores among all the experiments. It can be seen that combining all LPWs (GTS + LPW (HML)) results in a higher ETS than with conventional data for the entire period. Looking at the bold numbers, assimilating high PW results in the highest ETS from the 18- to 36-hr accumulated precipitation forecasts due to the moisture sensitivity in the radiances. Since both surface radiation and near-surface air radiation are very close (unless there is large contrast between the surface skin temperature and the surface air temperature) and they both are contained in the radiance observation, it is difficult to separate the surface contribution and the surface air contribution in the radiance observation from the water vapor absorption channel, and therefore, the moisture sensitivity to the radiance is low in the boundary layer, as studied by Di et al. (2016).

For ETS scores of rainfall greater than or equal to 10 mm, assimilating three-layered PW together (GTS + LPW (HML)) gives higher ETS scores than GTS only in the entire 48-hr forecast period. To study the impacts on heavy rainfall, the ETS, POD, and FAR scores of CNTRL and GTS + LPW (HML) for rainfall greater than or equal to 50 mm are calculated (Figure 4). Precipitation is accumulated with the forecasting time from 1200 UTC on 18 July. The ETS and POD scores are low during the first 6 hr, which indicates that accumulated precipitation of 50 mm rarely occurs during the first 6 hr. This is related to the model simulation for heavy precipitation, which is accumulated with the forecast time. In general, the POD and ETS of LPWs are higher than CNTRL, and the FAR of LPWs is slightly lower than CNTRL, which indicates that the assimilation of LPWs data can improve rainfall occurrences and reduce false positives. For the first 6-hr forecasts, both GTS and GTS + LPW (HML) have less heavy precipitation. Starting from the 12-hr forecasts, accumulated precipitation of more than 50 mm is evident for both experiments. While the ETS score for GTS + LPW (HML) is slightly lower than that for GTS alone at the 18-hr forecast, it is always higher than that of the GTS for the rest of the 48-hr forecast, especially from 36 to 48 hr. Assimilating AHI LPW (HML) adjusts the moisture fields of

Table 3
ETS Scores From All the Assimilation Experiments for Rainfall Greater Than or Equal to 10 mm Over Beijing 7.19/20 Storm

Experiment	Accumulated precipitation							
	6 hr	12 hr	18 hr	24 hr	30 hr	36 hr	42 hr	48 hr
ETS scores								
GTS	0.3241	0.5072	0.585	0.5234	0.497	0.4709	0.5028	0.525
GTS + LPW (H)	0.3101	0.4954	0.5937	0.5451	0.5242	0.507	0.5289	0.516
GTS + LPW (M)	0.3155	0.514	0.5729	0.5058	0.4918	0.4829	0.5098	0.5258
GTS + LPW (L)	0.3234	0.5234	0.5791	0.5243	0.493	0.4776	0.5062	0.5222
GTS + LPW (HM)	0.3119	0.5287	0.5887	0.5312	0.4858	0.4678	0.5008	0.5018
GTS + LPW (HL)	0.3327	0.519	0.5688	0.5203	0.4882	0.4722	0.4971	0.5042
GTS + LPW (ML)	0.3194	0.5112	0.5724	0.513	0.5039	0.4942	0.534	0.5531
GTS + LPW (HML)	0.3417	0.5258	0.5872	0.5244	0.5083	0.5006	0.5395	0.5585

Note. Numbers in bold indicate the highest ETS scores among all the experiments. ETS = equitable threat score; GTS = global telecommunication system; LPW = layered precipitable water.

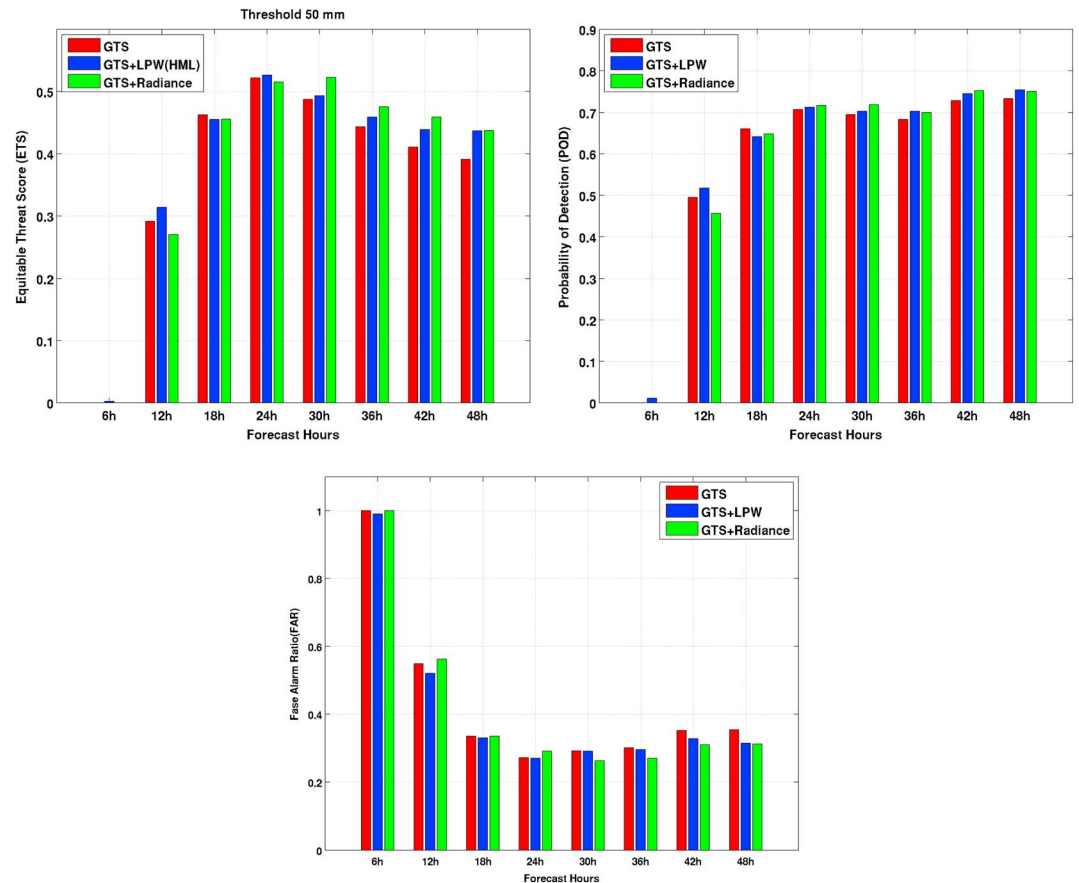


Figure 4. The ETS scores (upper left), POD (upper right) and FAR (lower panel) from GTS (red), GTS + LPW (HML) (blue) and GTS + radiance (green) for rainfall greater than or equal to 50 mm in case I, Beijing July 19/20, 2016 storm. GTS = global telecommunication system; LPW = layered precipitable water.

the analysis and can improve the precipitation forecast for heavy rainfall events more effectively than assimilating GTS conventional data alone.

3.3. Case II: Middle June 2016 Yangtze River Case

In mid-June 2016, heavy rainfall began across southern China, triggering deadly floods. Over the following month, additional rain events exacerbated the flooding, affecting more of the country. Areas along the Yangtze River and Huai-He River were particularly hard hit. A typical forecast case is selected for these assimilation experiments. The experiment's settings are similar to Case I, but the grid points are different. The outer domain (domain 1) has 400×300 grids, and the inner domain (domain 2) has 703×601 grids. Similar to Case I, the experiments start at 1800 UTC on 17 June 2016. After the 6-hr forecasts, the data are assimilated at 0000 UTC and 0600 UTC on 18 June and then followed by a 48-hr forecast. The assimilation window and observation error of LPW are the same as in Case I. Based on Case I, the GTS and GTS + LPW (HML) are used to study the impact of AHI LPW. The experiments are as follows:

1. CNTRL: GTS (conventional data)
2. GTS + LPW (HML) (conventional data + three-layered PW data from sigma level 0.3 to 0.7, from sigma level 0.7 to 0.9, and from sigma level 0.9 to 1.0)

Similar to Case I, the slope value (R) of the three-LPW products against background and analysis at 0000 and 0600 UTC on 18 June 2016 is calculated in Table 4. Based on the data distribution and the slope value, the slopes for high-level PW and low-level PW between the background and observations are larger than 1.0, which indicates that the background PW contains more moisture than the observations. On the contrary, the middle-level background PW is relatively drier than the observations. At both 0000 and 0600 UTC, after

Table 4
The Slope Number of Three-Layered Precipitable Water Against Background and Analysis at 0600 UTC on 18 June 2016

Slope	0000 UTC 18 June		0600 UTC 18 June	
	Background versus observation	Analysis versus observation	Background versus observation	Analysis versus observation
High PW	1.0041	0.99811	1.0161	0.99855
Middle PW	0.96586	0.99902	0.97901	0.99894
Low PW	1.0285	0.99926	1.0222	0.99909

Note. PW = precipitable water.

assimilation, the PW analyses are adjusted and they are closer to the observations (with slopes closer to 1.0) than the background. By comparing the background/analysis and the observations, it can be seen that the PW analyses have better agreement with the observations, which is also consistent with the results of Case I, the July Beijing storm.

To study the impact of assimilating LPW data on precipitation, the ETS scores are also calculated for the accumulated precipitation from the experiments. The precipitation from 23°N to 35°N latitude and from 105°E to 122°E longitude is used to calculate the ETS. Figure 5 shows the ETS scores with thresholds of 10, 20, 50, and 75 mm. The pattern of POD is consistent with the pattern of ETS scores (figure not shown). At the 10-mm precipitation threshold, the impacts from assimilating LPW data are mixed. But when the precipitation is greater than 20 mm, the impacts from assimilating LPW data are larger: the ETS scores for GTS + LPW (HML) are always larger than ETS scores for GTS after the 24-hr forecast, especially for precipitation greater than 50 and 75 mm. Figure 6 shows the ETS scores of accumulated precipitation from 0600 UTC on 18 June to 1200 UTC, 1800 UTC on 19 June, and 0000 and 0600 UTC on 20 June 2016. For light rainfall (< 10 mm),

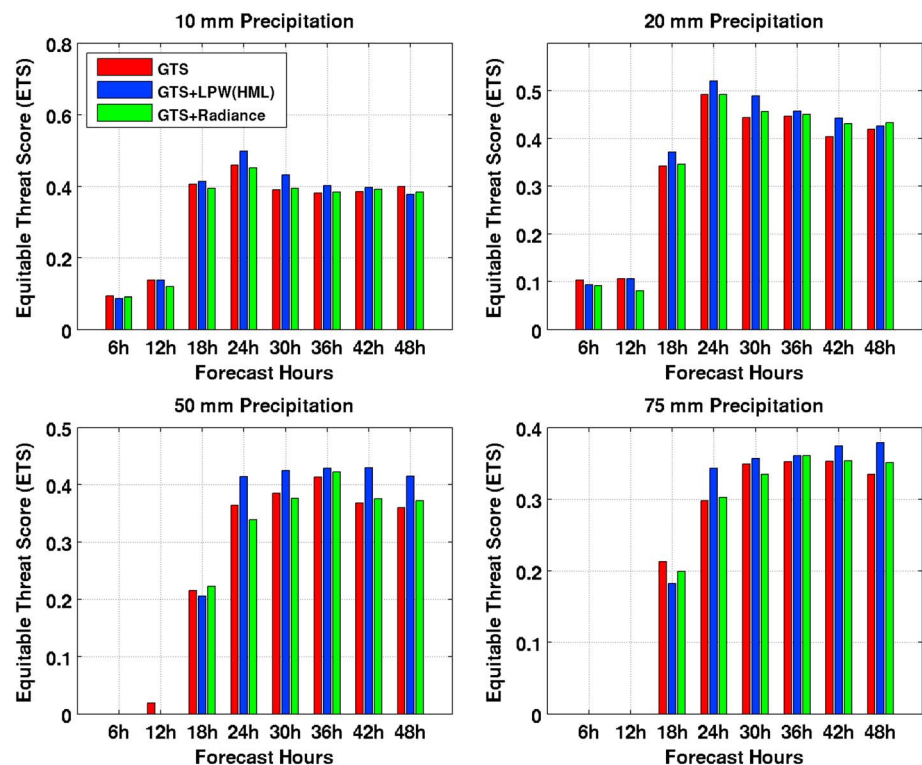


Figure 5. The ETS scores from GTS (red), GTS + LPW (HML) (blue) GTS + AHI (green) for 10-, 20-, 50-, and 75-mm rainfall threshold of Case II, mid-June 2016 Yangtze River Case. ETS = equitable threat score; GTS = global telecommunication system; LPW = layered precipitable water; AHI = Advanced Himawari Imager.

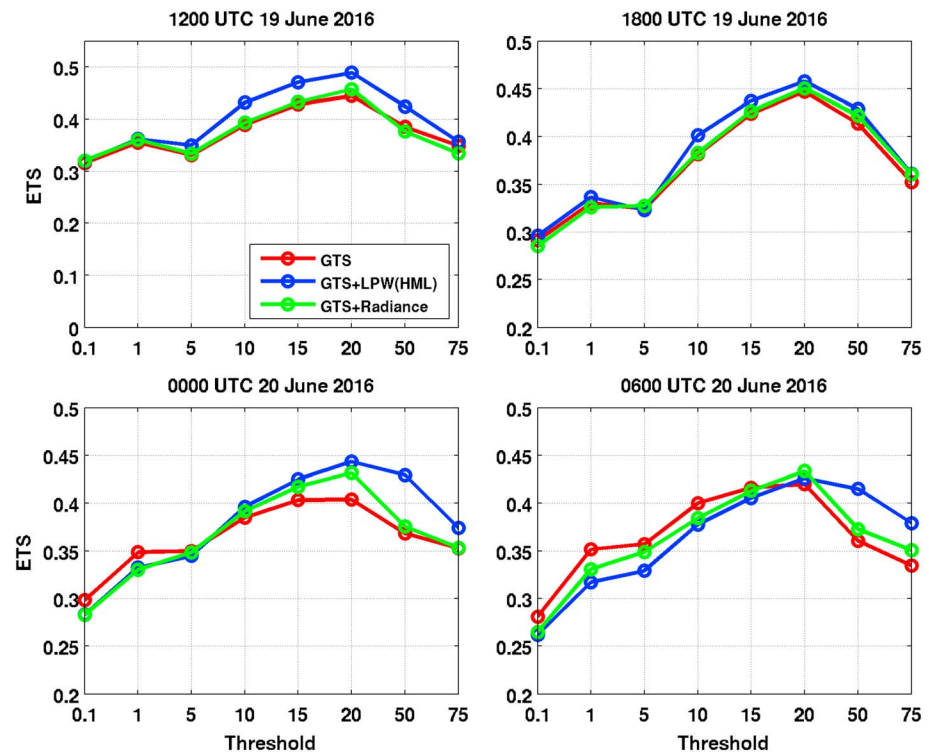


Figure 6. The ETS scores with threshold from 0.1 mm to 75 mm of GTS (red), GTS + LPW (HML) (blue), GTS + Radiance (green) at 1200 UTC, 1800 UTC on 19 June, 0000 UTC and 0600 UTC on 20 June 2016. ETS = equitable threat score; GTS = global telecommunication system; LPW = layered precipitable water; Radiance = Advanced Himawari Imager.

the ETS score for GTS + LPW (HML) is similar to or slightly smaller than the ETS score for GTS alone. However, when the precipitation is heavier and the forecast time is longer, the impacts of GTS + LPW (HML) become more significant. From the ETS scores for the two experiments from all forecasts, it can be seen that for rainfall less than 10 mm, adding LPWs does not significantly change the rainfall prediction; however, for rainfalls greater than 20 mm, adding AHIs LPWs can improve the forecasts, especially for very heavy rainfall (>50 mm) forecasts.

4. Comparison Between AHI Radiance Assimilation and LPW Assimilation

The LPW assimilation is different from the radiance assimilation. Assimilating LPW involves incorporating 1DVAR and 3DVAR into the process: in this case retrieving the LPWs with 1DVAR and assimilating them with 3DVAR (1DVAR/3DVAR system). Since the LPW retrieval process combines the information from the IR band radiances, global NWP background, and surface observations, the LPW has been demonstrated to be better than the global NWP (e.g., GFS) forecasts (Lee et al., 2014; Li et al., 2008, 2009). Even though a NWP background is used in the 1DVAR process, the background used in 1DVAR is different from the background in the assimilation. For example, 1DVAR uses global NWP 9- to 12-hr forecasts as the background, while 3DVAR uses the regional NWP fields as the background.

To assimilate the AHI radiance data, the GSI-v3.5 3DVAR system is used and has the capability to directly assimilate AHI radiances. The thinning box for AHI radiances is 60 km. In the radiance assimilation, radiances from IR bands 8–10 and 16 are used in the assimilation over both ocean and land regions. Those bands are also used in the LPW retrieval process. An enhanced bias correction method is applied for AHI radiances bias correction (Zhu et al., 2014). Figure 7 shows the AHI BT of bands 8, 9, and 10 for observation, background, and analysis at 0000 UTC on 18 June 2016. The cold bias is removed after bias correction. For band 8, the bias is adjusted from 0.5516 to 0.021 K, and for band 9 the bias is adjusted from 0.933 to 0.0038 K after bias correction. The standard deviations (STD) for all three channels are reduced with bias correction. The BTs of the analysis fields are much closer to the observations with a significant reduction in STD from the background.

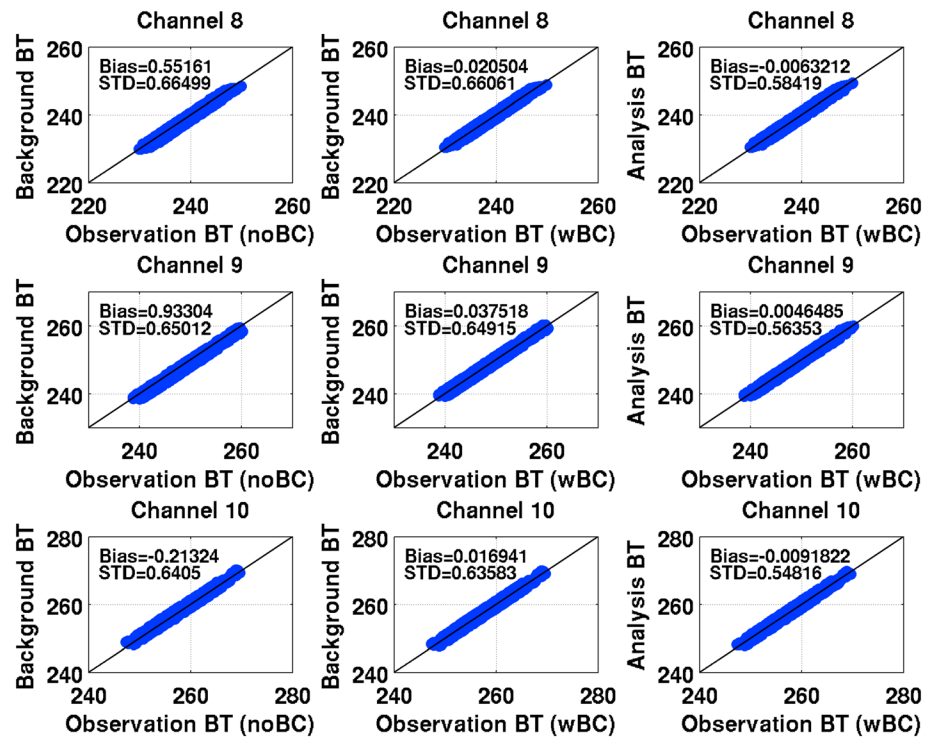


Figure 7. The brightness temperature (K) of AHI observation, background, and analysis of channels 8, 9, and 10 at 0600 UTC on 18 June 2016. The simulated AHI brightness temperatures from background without bias correction (noBC) are in the left column, with bias correction (wBC) are in middle column, and from the analysis are in the right column. The bias and standard deviation are marked in each figure. AHI = Advanced Himawari Imager; STD = standard deviation.

The AHI radiances are assimilated for both Cases I and II, and all of the NWP model settings are the same as in section 3.3. In addition to the ETS scores from GTS and GTS + LPW (HML), the ETS scores from GTS + Radiance are also shown in green in Figures 4–6. From the ETS scores, it can be seen that for the light rain in Case II, the ETS for GTS + Radiance is comparable to that for GTS. For the 20-mm precipitation threshold, the assimilation of GTS + Radiance is higher than that for GTS but slightly lower than that for GTS + LPW (HML). For heavy precipitation (> 50 mm), the ETS for GTS + LPW (HML) is higher than GTS after the 24-hr forecast, and the ETS for GTS + Radiance is higher than the ETS for GTS after the 36-hr forecast. Relative to GTS, GTS + LPW (HML) has the most positive impact for long period heavy precipitation forecast. For Case I, the ETS scores for heavy precipitation (Figure 4 upper left) for both GTS + LPW and GTS + Radiance are higher than the ETS for GTS only after the 30-hr forecast. The results for GTS + LPW and GTS + Radiance are mixed at different periods, though they are comparable. The POD and FAR scores have a similar pattern. Results from these two cases indicate that adding LPW (HML) and AHI Radiances has a larger impact for heavy precipitation forecasts over land.

The upper panel of Figure 8 shows the mixing ratio of the background, and the lower panel of Figure 8 shows an example of the assimilated observation data coverage of AHI radiances (channel 9, green squares) and high PW (red stars) over a BT image of AHI channel 14 (shaded) at 0600 UTC on 18 June 2016 (Case II). AHI channel 14 is a window channel which can provide high-resolution cloud information; therefore, it is used as background in Figure 8 (note that the channel 14 is not assimilated). For both radiances and LPW data, the assimilated observations are under clear-sky conditions. For the region from 25°N to 29°N latitude and from 105°E to 110°E longitude, the high-PW data are assimilated but radiances are not assimilated. These regions are under clear skies. Based on the mixing ratio over this area (upper panel of Figure 8), the mixing ratio is over 10 g/kg. Therefore, the lack of radiance assimilation at this region might result in a reduction of the information needed on the mixing ratio. For the region from 25°N to 28°N latitude and from 110°E to 120°E longitude, the radiances are assimilated in some locations. However, these regions are affected by

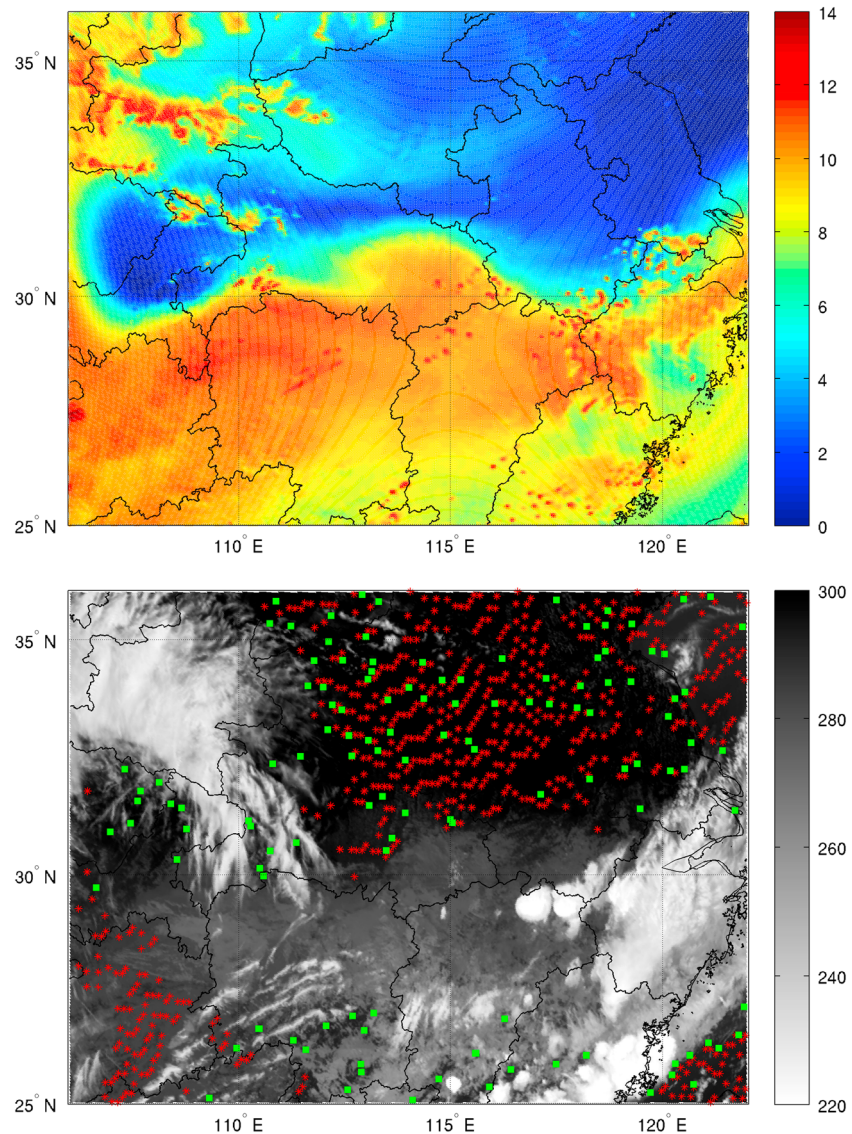


Figure 8. The mixing ratio (upper, unit: g/kg) from background at 700 hPa and the assimilated radiances of AH channel 9 (lower, green squares), the assimilated high-layer PW (lower, red stars), and the brightness temperature of AH channel 14 (lower shaded, unit: K) at 0600 UTC on 18 June 2016. AH = Advanced Himawari Imager; PW = precipitable water

Table 5

The Number of Assimilated AH Radiances Over Ocean and Over Land for IR Band 8–10 and 16 at 0600 UTC on 18 June 2016

IR channel	0000 UTC 18 June		0600 UTC 18 June	
	Over ocean	Over land	Over ocean	Over land
Ch 8	1,018	812	933	608
Ch 9	1,054	829	903	593
Ch 10	1,138	878	977	659
Ch 16	1,245	836	1,064	531

Note. IR = infrared.

clouds based on data from AH channel 14. The cloud contamination might degrade the impact of the radiance assimilation.

The differences in data coverage outlined above could be caused by the cloud detection method used by the two data assimilation methods. In the GSI radiance assimilation, clear sky is based on the differences between the background (or first guess) fields, which is from the model simulation, and the observations. There are often mismatches. For example, the model may indicate clear skies but observations may indicate clouds, and vice versa. In these situations the differences are generally large and the observations are easily removed as outliers as shown in the lower left of Figure 8 in the lower panel. There is another opposite situation in which the difference is small, and the observation is brought in for assimilation, but actually the observation indicates

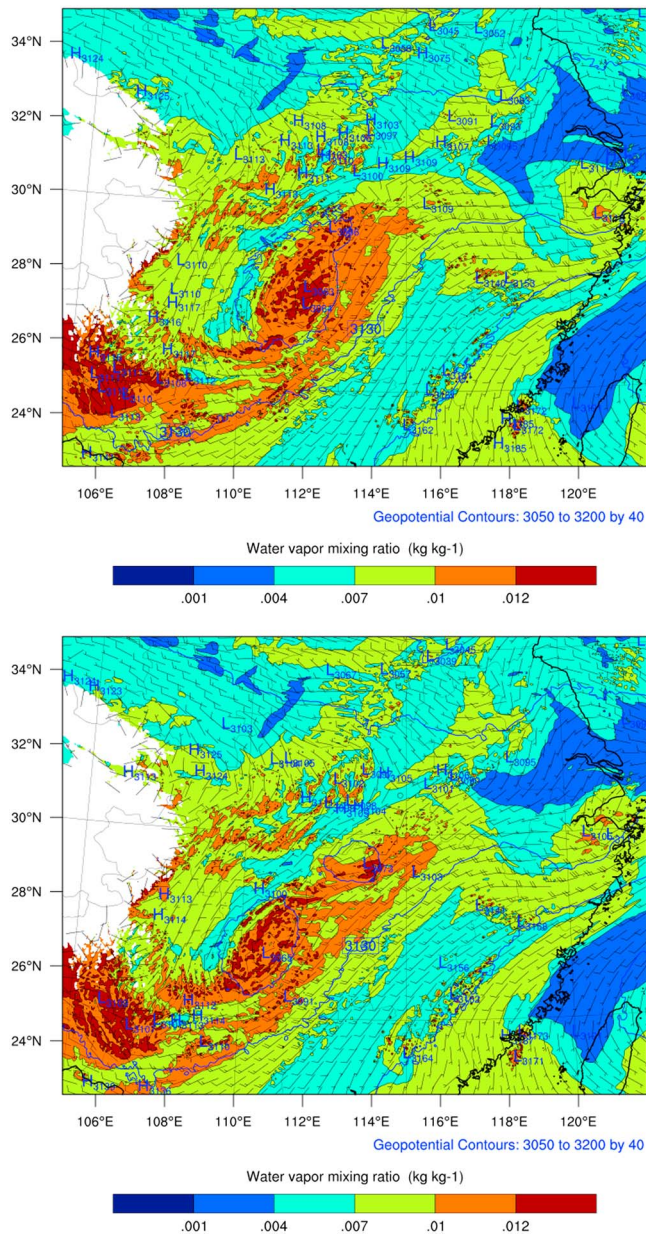


Figure 9. The geopotential height (blue solid line, m^2/s^2), water vapor mixing ratio (shaded, kg/kg), and winds (vector) at 700 hPa of GTS + LPW (HML) (upper panel) and GTS + Radiance (lower panel) at 0600 UTC on 20 June 2016. GTS = global telecommunication system; LPW = layered precipitable water.

cloudy skies (shown in the lower middle of Figure 8 lower panel). The cloud-contaminated radiance might degrade the impact of the radiance assimilation. Because the LPW algorithm uses observations only for cloud detection, it does not have a mismatch problem. In other regions, the patterns of observations assimilated in the two experiments are similar. The numbers of assimilated AHI radiances over ocean and over land for each IR band are listed in Table 5, with the numbers of assimilated radiances over land being smaller than those over ocean in this case. The IR surface emissivity uncertainty and the complicated topography over land make the radiance difficult to use. Figure 9 shows the water vapor mixing ratio and winds from (a) GTS + LPW (HML) and (b) GTS + Radiance at the 48-hr forecasts. In general, the mixing ratio of GTS + Radiance is slightly drier than that of GTS + LPW (HML), especially in the region around 27°N latitude and 112°E longitude. The limited radiances assimilated over land affect the atmospheric fields and the precipitation forecasts. Unlike Case II, the observations from LPWs and radiances are more evenly distributed and assimilated data points are closer in Case I, which may be one of the reasons that the results for the two experiments are mixed and more comparable. The high-quality observational information from either radiances or LPWs is very important to improve the heavy precipitation forecast.

In addition to the cloud detection difference, there are also other possible reasons or factors that affect the different results from LPW assimilation and radiance assimilation: (1) Methods are different as mentioned above. The radiance assimilation is based on 3DVAR in our studies, and it handles nonlinearity during the assimilation process, while the LPW assimilation is based on the combination of 1DVAR/3DVAR, and it handles the nonlinearity mainly during the 1DVAR retrieval stage. (2) In the regional NWP data assimilation, when the atmosphere is wet, the Jacobian might still have value above the model top, while the LPW assimilation does not exhibit this concern. (3) Handling surface IR emissivity is different in radiance assimilation and LPW assimilation. Emissivity is assumed to be known in the radiance assimilation, while emissivity is retrieved together with the LPW in the 1DVAR process. According to Migliorini (2012) both radiance and LPW assimilation can be used: Theoretically, there is equivalence between radiance and retrieval assimilation under certain circumstances, which is demonstrated, in part, by the experiments in this study. The purpose of these comparisons between LPW and radiance assimilation is to study an alternative way of assimilating the important AHI moisture information into NWP. The 1DVAR processor can be implemented in the geostationary satellite data processing package for near-real-time LPW generation, and it is relatively straightforward to assimilate LPW in regional NWP (e.g., easier forward operator and no data format conversion).

5. Summary and Discussion

The forward operator for LPWs has been developed and implemented in the GSI 3DVAR for assimilating the three LPWs from AHI. AHI LPWs are produced at SSEC by using a 1Dvar algorithm similar to that which was developed for GOES-R ABI. AHI moisture information assimilation experiments were conducted with a regional-/storm-scale NWP model, and the impact of assimilating LPW on precipitation forecasts of two heavy rainfall events in China during 2016 is discussed in this study. In addition, the impact of assimilating clear-sky AHI IR radiances is tested for the case study. Overall, AHI moisture assimilation has a positive impact on LSS forecasts, especially for heavy rainfall forecasts. Upper tropical moisture in the environment is very

important to the assimilation for precipitation forecasts, which is consistent with findings from assimilating the current GOES Sounder LPWs over contiguous United States for LSS forecasts (not shown).

Although IR radiance assimilation has been demonstrated successfully at most operational centers, assimilating LPW is studied as an alternative approach for assimilating moisture information from advanced imagers onboard the new generation of geostationary weather satellites. Despite the difficulty of comparison, the experiments show that overall LPW assimilation and radiance assimilation provide similar or comparable precipitation forecasts. Two points affect the assimilation and forecast results. The first is the different approaches in cloud detection as discussed in last section. Due to its dependence on the background fields, the GSI radiance approach could have mismatches and cloud contamination, which may either miss some good observations or degrade the radiance assimilation impact. The second point is that the surface IR emissivity uncertainty and complicated topography will limit the radiance assimilation. In addition, the methods of handling nonlinearity during the assimilation process are different. The purpose of these comparisons between LPW and radiance assimilation is to study an alternative way of assimilating the important AHI moisture information into NWP.

The AHI/ABI will provide key information related to high temporal and spatial resolution moisture in the environment of LSS. While there will be no hyperspectral IR sounder on the GOES-R series to provide more accurate vertical temperature and moisture information, an important benefit to regional NWP model applications and AHI/ABI's high spatiotemporal resolutions makes it possible to employ it for severe storm nowcasting and short-range forecasting. The AHI/ABI spatial resolution of 2 km (IR channels) is not available from any other satellite measurements, thus making it useful for preconvective moisture observations. The temporal resolutions of 30 s in the mesoscale, 5 min over the contiguous United States, and 15 min over the full disk also provide unprecedented measurements that could capture the rapid evolution of convective situations which is useful for short-term, severe storm forecasts. The assimilation of liquid and ice water path retrievals from the GOES Imager shows improvement of thermodynamic conditions at the surface layer (Jones et al., 2016). Taking full advantage of high spatial and temporal resolution in the regional-/storm-scale model will be the focus of future work.

Another important future study is the assimilation of cloudy radiances. Normally, only clear radiances (not affected by clouds) or limited radiances in cloudy skies are used in most data assimilation systems, and cloud-affected data have not been used effectively due to difficulties in modeling clouds in both forecast and radiative transfer models (Li et al., 2016). Retrieving LPW under cloudy skies has been investigated, with results showing that in some cloudy situations, such as lower clouds or thin clouds, the upper tropospheric LPW can also improve the GFS background (Li et al., 2009). Utilizing LPW in cloudy regimes has been shown to be very useful to local forecasters, which was demonstrated successfully during the 2015 and 2016 Hazardous Weather Testbed spring experiments (<http://goesrhwt.blogspot.com/search/label/GOES-R%20LAP>), but has not yet been tested for impacts in NWP. In addition, how to better use the surface emissivity database in both LPW retrieval and radiance assimilation is also an important research topic. The accurately described surface types and surface emissivity is one of the most important factors for assimilating surface sensitive channels.

The focus of this paper is on the assimilation of LPWs and demonstrating the value-added impact from LPW assimilation on heavy precipitation forecasts over that from assimilating conventional data only, as well as the comparisons between LPW assimilation and direct radiance assimilation. Future work will also include other information such as IR and MW sounder data from polar orbiting satellites, as well as atmospheric motion vectors from GEO.

Acknowledgments

This work was supported by NOAA GOES-R series algorithm working group (AWG), Risk Reduction, high impact weather (HIW) and NSF 41775045 programs. We appreciate support from the CIMSS/SSEC sounding team in preparing the AHI LPWs data and the SSEC Data Center for providing the AHI radiance data (<http://www.ssec.wisc.edu/data/>). The authors would like to thank Agnes Lim who helped convert and assimilate the AHI radiance data in the GSI system. The precipitation observation data can be found at <http://cdc.cma.gov.cn/sksj.do?method=ssrjscpnh>. The FNL reanalysis data and GTS data can be downloaded from the NCAR/UCAR Research Data Archive (<https://rda.ucar.edu/datasets/>). The views, opinions, and findings contained in this report are those of the authors and should not be construed as an official National Oceanic and Atmospheric Administration or U.S. Government position, policy, or decision. The official website for the GOES-R series mission is <http://www.goes-r.gov>.

References

- Bessho, K., Date, K., Hayashi, M., Ikeada, A., Imai, T., Inoue, H., et al. (2016). An introduction to Himawari-8/9—Japan's new-generation geostationary meteorological satellites. *Journal of the Meteorological Society of Japan*, 94(2), 151–183. <https://doi.org/10.2151/jmsj.2016-009>
- Boukabara, S., Zhu, T., Tolman, H., Lord, S., Goodman, S., Atlas, R., et al. (2016). S4: An O2R/R2O infrastructure for optimizing satellite data utilization in NOAA numerical modeling systems: A step toward bridging the gap between research and operations. *Bulletin of the American Meteorological Society*, 97(12), 2359–2378. <https://doi.org/10.1175/BAMS-D-14-00188.1>
- Chen, Y., Han, Y., Van Delst, P., & Weng, F. (2010). On water vapor Jacobian in fast radiative transfer model. *Journal of Geophysical Research*, 115, D12303. <https://doi.org/10.1029/2009JD013379>

- Chen, Y., Han, Y., & Weng, F. (2012). Comparison of two transmittance algorithms in the community radiative transfer mode: Application to AVHRR. *Journal of Geophysical Research*, *117*, D06206. <https://doi.org/10.1029/2011JD016656>
- Deblonde, G. (1999). Variational assimilation of SSM/I total precipitable water retrievals in the CMC analysis system. *Monthly Weather Review*, *127*(7), 1458–1476. [https://doi.org/10.1175/1520-0493\(1999\)127%3C1458:VAOSIT%3E2.0.CO;2](https://doi.org/10.1175/1520-0493(1999)127%3C1458:VAOSIT%3E2.0.CO;2)
- Di, D., Ai, Y., Li, J., Shi, W., & Lu, N. (2016). Geostationary satellite-based 6.7 μm band best water vapor information layer analysis over the Tibetan Plateau. *Journal of Geophysical Research: Atmospheres*, *121*, 4600–4613. <https://doi.org/10.1002/2016JD024867>
- Ebert, E. E., Janowiak, J. E., & Kidd, C. (2007). Comparison of near-real-time precipitation estimates from satellite observations and numerical models. *Bulletin of the American Meteorological Society*, *88*(1), 47–64. <https://doi.org/10.1175/BAMS-88-1-47>
- Hamill, T. M. (1999). Hypothesis tests for evaluating numerical precipitation forecasts. *Weather and Forecasting*, *14*(2), 155–167. [https://doi.org/10.1175/1520-0434\(1999\)014%3C0155:HTFENP%3E2.0.CO;2](https://doi.org/10.1175/1520-0434(1999)014%3C0155:HTFENP%3E2.0.CO;2)
- Han, H.-J., Li, J., Goldberg, M., Wang, P., Li, J., Li, Z., et al. (2016). Microwave sounder cloud detection using a collocated high resolution imager and its impact on radiance assimilation in tropical cyclone forecasts. *Monthly Weather Review*, *144*, 3927–3959.
- Han, Y., Van Delst, P., Liu, Q., Weng, F., Yan, B., Treadon, R., & Derber, J. (2006). JCSDA Community Radiative Transfer Model (CRTM)—Version 1, NOAA Tech Report 122.
- Heidinger, A. K., Foster, M. J., Walther, A., & Zhao, X. (2013). The Pathfinder Atmospheres Extended (PATMOS-x) AVHRR Climate Data Set. *Bulletin of the American Meteorological Society*. <https://doi.org/10.1175/BAMS-D-12-00246.1>
- Hong, S.-Y., & Lim, J.-O. J. (2006). The WRF single-moment 6-class microphysics scheme (WSM6). *Journal of Korean Meteorological Society*, *42*(2), 129–151.
- Hong, S. Y., Noh, Y., & Dudhia, J. (2006). A new vertical diffusion package with an explicit treatment of entrainment processes. *Monthly Weather Review*, *134*(9), 2318–2341. <https://doi.org/10.1175/MWR3199.1>
- Hou, A. Y., Ledvina, D. V., Da Silva, A. M., Zhang, S. Q., Joiner, J., Atlas, R. M., et al. (2000). Assimilation of SSM/I-derived surface rainfall and total precipitable water for improving the GEOS analysis for climate studies. *Monthly Weather Review*, *128*(3), 509–537. [https://doi.org/10.1175/1520-0493\(2000\)128%3C0509:AOSIDS%3E2.0.CO;2](https://doi.org/10.1175/1520-0493(2000)128%3C0509:AOSIDS%3E2.0.CO;2)
- Iacono, M. J., Delamere, J. S., Mlawer, E. J., Shephard, M. W., Clough, S. A., & Collins, W. D. (2008). Radiative forcing by long-lived greenhouse gases: Calculations with the AER radiative transfer models. *Journal of Geophysical Research*, *113*, D13103. <https://doi.org/10.1029/2008JD009944>
- Jin, X., Li, J., Schmit, T. J., Li, J., Goldberg, M. D., & Gurka, J. J. (2008). Retrieving clear-sky atmospheric parameters from SEVIRI and ABI infrared radiances. *Journal of Geophysical Research: Atmospheres*, *113*, D15310. <https://doi.org/10.1029/2008JD010040>
- Jones, T. A., Knopfmeier, K., Wheatley, D., Creager, G., Minnis, P., & Palikonda, R. (2016). Storm-scale data assimilation and ensemble forecasting with the NSSL experimental warn-on-forecast system. Part II: Combined radar and satellite data experiments. *Weather and Forecasting*, *31*(1), 297–327. <https://doi.org/10.1175/WAF-D-15-0107.1>
- Kain, J. S. (2004). The Kain-Fritsch convective parameterization, 2004: An update. *Journal of Applied Meteorology*, *43*(1), 170–181. [https://doi.org/10.1175/1520-0450\(2004\)043%3C0170:TKCPAU%3E2.0.CO;2](https://doi.org/10.1175/1520-0450(2004)043%3C0170:TKCPAU%3E2.0.CO;2)
- Kleist, D. T., Parrish, D. F., Derber, J. C., Treadon, R., Wu, W.-S., & Lord, S. (2009). Introduction of the GSI into the NCEP global data assimilation system. *Weather and Forecasting*, *24*(6), 1691–1705. <https://doi.org/10.1175/2009WAF2222201.1>
- Lee, Y.-K., Li, J., Li, Z., & Schmit, T. J. (2017). Atmospheric temporal variations in the pre-landfall environment of Typhoon Nangka (2015) observed by the Himawari-8 AHI. *Asia-Pacific Journal of Atmospheric Sciences*, 1976–7633. <https://doi.org/10.1007/s13143-017-0046-z>
- Lee, Y.-K., Li, Z., Li, J., & Schmit, T. J. (2014). Evaluation of the GOES-R ABI LAP retrieval algorithm using GOES-13 Sounder. *Journal of Atmospheric and Oceanic Technology*, *31*(1), 3–19. <https://doi.org/10.1175/JTECH-D-13-00028.1>
- Li, J., Li, J., Otkin, J., Schmit, T. J., & Liu, C. (2011). Warning information in a preconvective environment from the geostationary advanced infrared sounding system—A simulation study using IHOP case. *Journal of Applied Meteorology and Climatology*, *50*(3), 776–783. <https://doi.org/10.1175/2010JAMC2441.1>
- Li, J., Liu, C.-Y., Zhang, P., & Schmit, T. J. (2012). Applications of full spatial resolution space-based advanced infrared soundings in the preconvective environment. *Weather and Forecasting*, *27*(2), 515–524. <https://doi.org/10.1175/WAF-D-10-05057.1>
- Li, J., & Liu, H. (2009). Improved hurricane track and intensity forecast using single field-of-view advanced IR sounding measurements. *Geophysical Research Letters*, *36*, L11813. <https://doi.org/10.1029/2009GL038285>
- Li, J., Wang, P., Han, H., Li, J., & Zheng, J. (2016). On the assimilation of satellite sounder data in cloudy skies in the numerical weather prediction models. *Journal of Meteorological Research*, *30*(2), 169–182. <https://doi.org/10.1007/s13351-016-5114-2>
- Li, J., Wolf, W., Menzel, W. P., Zhang, W., Huang, H.-L., & Achtor, T. H. (2000). Global soundings of the atmosphere from ATOVS measurements: The algorithm and validation. *Journal of Applied Meteorology*, *39*(8), 1248–1268. [https://doi.org/10.1175/1520-0450\(2000\)039%3C1248:GSOTAF%3E2.0.CO;2](https://doi.org/10.1175/1520-0450(2000)039%3C1248:GSOTAF%3E2.0.CO;2)
- Li, Z., Li, J., Menzel, W. P., Nelson, J. P. III, Schmit, T. J., Weisz, E., & Ackerman, S. A. (2009). Forecasting and nowcasting improvement in cloudy regions with high temporal GOES Sounder infrared radiance measurements. *Journal of Geophysical Research: Atmospheres*, *114*, D09216. <https://doi.org/10.1029/2008JD010596>
- Li, Z., Li, J., Menzel, W. P., Schmit, T. J., Nelson, J. P. III, Daniels, J., & Ackerman, S. A. (2008). GOES sounding improvement and applications to severe storm nowcasting. *Geophysical Research Letters*, *35*, L03806. <https://doi.org/10.1029/2007GL032797>
- Lim, A. H. N., Jung, J. A., Huang, H.-L. A., Ackerman, S. A., & Otkin, J. A. (2014). Assimilation of clear sky atmospheric infrared sounder radiances in short-term regional forecasts using community models. *Journal of Applied Remote Sensing*, *8*, 083655–1–083655-27. <https://doi.org/10.1117/1.JRS.8.083655>
- Liu, H., & Li, J. (2010). An improved in forecasting rapid intensification of Typhoon Sinlaku (2008) using clear-sky full spatial resolution advanced IR soundings. *Journal of Applied Meteorology and Climatology*, *49*(4), 821–827. <https://doi.org/10.1175/2009JAMC2374.1>
- Ma, Z., Maddy, E. S., Zhang, B., Zhu, T., & Boukabara, S. A. (2017). Impact assessment of Himawari-8 AHI data assimilation in NCEP GDAS/GFS with GSI. *Journal of Atmospheric and Oceanic Technology*, *34*(4), 797–815. <https://doi.org/10.1175/JTECH-D-16-0136.1>
- Migliorini, S. (2012). On the equivalence between radiance and retrieval assimilation. *Monthly Weather Review*, *140*(1), 258–265. <https://doi.org/10.1175/MWR-D-10-05047.1>
- Qin, Z., Zou, X., & Weng, F. (2013). Evaluating added benefits of assimilating GOES imager radiance data in GSI for coastal QPFs. *Monthly Weather Review*, *141*(1), 75–92. <https://doi.org/10.1175/MWR-D-12-00079.1>
- Qin, Z., Zou, X., & Weng, F. (2017). Impacts of assimilating all or GOES-like AHI infrared channels radiances on QPFs over Eastern China. *Tellus*, *69*(1), 1345265. <https://doi.org/10.1080/16000870.2017.1345265>
- Rakesh, V., Singh, R., Pal, P. K., & Joshi, P. C. (2009). Impacts of satellite-observed winds and total precipitable water on WRF short-range forecasts over the Indian region during the 2006 summer monsoon. *Weather and Forecasting*, *24*(6), 1706–1731. <https://doi.org/10.1175/2009WAF2222242.1>

- Schmit, T. J., Griffith, P., Gunshor, M. M., Daniels, J. M., Goodman, S. J., & Lebair, W. J. (2017). A closer look at the ABI on GOES-R. *Bulletin of the American Meteorological Society*, *98*, 681–698.
- Schmit, T. J., Gunshor, M. M., Menzel, W. P., Gurka, J., Li, J., & Bachmeier, S. (2005). Introducing the next-generation advanced baseline imager (ABI) on GOES-R. *Bulletin of the American Meteorological Society*, *86*(8), 1079–1096. <https://doi.org/10.1175/BAMS-86-8-1079>
- Schmit, T. J., Li, J., Gurka, J. J., Goldberg, M. D., Schrab, K., Li, J., & Feltz, W. (2008). The GOES-R advanced baseline imager and the continuation of current GOES sounder products. *Journal of Applied Meteorology and Climatology*, *47*(10), 2696–2711. <https://doi.org/10.1175/2008JAMC1858.1>
- Shen, Y., Zhao, P., Pan, Y., Yu, J. J., & J. J. (2014). A high spatiotemporal gauge-satellite merged precipitation analysis over China. *Journal of Geophysical Research: Atmospheres*, *119*, 3063–3075. <https://doi.org/10.1002/2013JD020686>
- Sieglauff, J. M., Schmit, T. J., Menzel, W. P., & Ackerman, S. A. (2009). Inferring convective weather characteristics with geostationary high spectral resolution IR window measurements: A look into the future. *Journal of Atmospheric and Oceanic Technology*, *26*(8), 1527–1541. <https://doi.org/10.1175/2009JTECHA1210.1>
- Wang, P., Li, J., Goldberg, M. D., Schmit, T. J., Lim, A. H. N., Li, Z., & Ackerman, S. A. (2015). Assimilation of thermodynamic information from advanced infrared sounders under partially cloudy skies for regional NWP. *Journal of Geophysical Research: Atmospheres*, *120*, 5469–5484. <https://doi.org/10.1002/2014JD022976>
- Wang, P., Li, J., Li, J., Li, Z., Schmit, T. J., & Bai, W. (2014). Advanced infrared sounder subpixel cloud detection with imagers and its impact on radiance assimilation in NWP. *Geophysical Research Letters*, *41*, 1773–1780. <https://doi.org/10.1002/2013GL059067>
- Wang, X., Parrish, D., Kleist, D., & Whitaker, J. (2013). GSI 3DVar-based ensemble-variational hybrid data assimilation for NCEP global forecast system: Single-resolution experiments. *Monthly Weather Review*, *141*(11), 4098–4117. <https://doi.org/10.1175/MWR-D-12-00141.1>
- Weisz, E., Smith, N., & Smith, W. L. (2015). The use of hyperspectral sounding information to monitor atmospheric tendencies leading to severe local storms. *Earth and Space Science*, *2*, 369–377. <https://doi.org/10.1002/2015EA000122>
- Wu, W.-S., Purser, R. J., & Parrish, D. F. (2002). Three-dimensional variational analysis with spatially inhomogeneous covariances. *Monthly Weather Review*, *115*, 209–232.
- Yang, J., Zhang, Z., Wei, C., Lu, F., & Guo, Q. (2017). Introducing the new generation of Chinese geostationary weather satellites—FengYun 4 (FY-4). *Bulletin of the American Meteorological Society*, *98*, 1637–1658.
- Zhang, F., Minamide, M., & Clothiaux, E. E. (2016). Potential impacts of assimilating all-sky infrared satellite radiances from GOES-R on convection-permitting analysis and prediction of tropical cyclones. *Geophysical Research Letters*, *43*, 2954–2963. <https://doi.org/10.1002/2016GL068468>
- Zhu, Y., Derber, J., Collard, A., Dee, D., Treadon, R., Gayno, G., & Jung, J. A. (2014). Enhanced radiance bias correction in the National Centers for Environmental Prediction's Gridpoint Statistical Interpolation data assimilation system. *Quarterly Journal of the Royal Meteorological Society*, *240*(682), 1479–1492.
- Zou, X., Qin, Z., & Weng, F. (2011). Improved coastal precipitation forecasts with direct assimilation of GOES-11/12 imager radiances. *Monthly Weather Review*, *139*(12), 3711–3729. <https://doi.org/10.1175/MWR-D-10-05040.1>